Isothermal and Nonisothermal Crystallization of Poly(aryl ether ketone ketone) with All-*para* Phenylene Linkage

JIKU WANG, XIAONIU YANG, GAO LI, ENLE ZHOU

State Key Laboratory of Polymer Physics and Chemistry, Changchun Institute of Applied Chemistry, Chinese Academy of Sciences, Changchun 130022, People's Republic of China

Received 2 January 2001; accepted 1 February 2001

ABSTRACT: Isothermal and nonisothermal crystallization behavior for PEKK(T) was studied using differential scanning calorimetry (DSC), transmission electron microscopy (TEM), and electron diffraction (ED). In the isothermal crystallization process, the Avrami parameters obtained were $n = 2.33–2.69$, which shows crystal growth of two-dimensional extensions consistent with our observations by TEM. The lamellar thickness increases with the crystallization temperature of PEKK(T) crystallized isothermally from the melt. However, for the nonisothermal crystallization of PEKK(T), the results from the modified Avrami analysis show two different crystallization processes. Avrami exponents $n_1 = 3.61–5.30$, obtained from the primary crystallization process, are much bigger than are the secondary $n_2 = 2.26–3.04$ and confirmed by the observation of the spherulite morphology. PEKK(T) crystallized isothermally from the melt possesses the same crystal structure (Form I) as that from nonisothermal melt crystallization. The results from TEM observation show that the spherulite radius decreases with an increasing cooling rate. © 2001 John Wiley & Sons, Inc. J Appl Polym Sci 82: 3431–3438, 2001

Key words: poly(ether ketones); crystallization; kinetics; morphology

INTRODUCTION

Poly(aryl ether ketone)s are very important engineering thermoplastics. As one member of this family, poly(aryl ether ketone ketone) with all-*para* phenylene linkages [PEKK(T)] receives more attention because of its polymorphism, Form I and Form II. The two forms are both orthohombic unit cells containing two molecular chains, and their unit cell dimensions are, respectively, Form I: $a = 0.776$ nm, $b = 0.606$ nm, $c = 1.008$ nm, and Form II: $a = 0.419$ nm, $b = 1.134$ nm, $c = 1.008$ nm.[1–3] Generally, the pure Form I can be obtained by isothermal crystallization from the melt above the temperature of 310°C, and the pure Form II, by cold crystallization from the glassy state at 180–220°C, after being quenched by liquid nitrogen, or by solvent-induced crystallization in a method in which film samples have been exposed to a CH_2Cl_2 atmosphere for 1 week.[4–6]

In this article, the isothermal and nonisothermal crystallization behavior of Form I of PEKK(T) from the Avrami equation, by DSC, and from morphology observation by transmission electron microscopy (TEM) are discussed. Meantime, analysis is also made by comparing the results from crystallization kinetics with those from TEM morphology observations.

Correspondence to: G. Li (ydh@ns.ciac.jl.cn).

Contract grant sponsors: State Science and Technology Commission of China; National Natural Science Foundation of China for Funding; Special Funds for Major State Research Projects.

Journal of Applied Polymer Science, Vol. 82, 3431–3438 (2001)

EXPERIMENTAL

Materials and Preparation

The samples of PEKK(T) were provided by Stephen Z. D. Cheng, and its number average weight is 7000–10,000. The chemical structure of PEKK(T) is as follows:

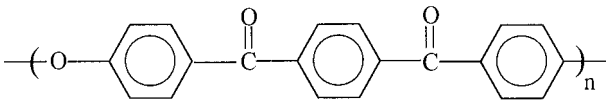

Differential Scanning Calorimetry

Isothermal and nonisothermal crystallization kinetics were carried out using a Perkin–Elmer DSC-7 differential scanning calorimeter calibrated for temperature with indium. All DSC tests were performed under a nitrogen purge; sample weights were between 8 and 10 mg.

Isothermal and Nonisothermal Crystallization Process

The samples were heated at a rate of 80°C/min to 20°C above the equilibrium melting temperature of PEKK(T) (410°C) for 5 min, then rapidly cooled to a predetermined temperature for isothermal crystallization or cooled at a different cooling rate for nonisothermal crystallization.

Sample Preparation for TEM

Thin films were prepared by casting a 0.05% PEKK(T)–pentafluorophenol (PFP) (w/w) solution at about 80°C onto freshly cleaved mica plates coated with carbon and then evaporated in a vacuum oven. The films were heated to 20°C above the equilibrium melting point (410°C) of PEKK(T) and then rapidly cooled to the designed temperature for isothermal crystallization or cooled at a designed cooling rate for nonisothermal crystallization. Afterward, the film was floated off the mica substrate on the water and then picked up using copper grids. The PEKK(T) crystal morphology and electron diffraction (ED) patterns were observed via a JEOL-2010 TEM using a 200-kV accelerating voltage. The PEKK(T) films were shadowed by Pt/Au and coated with carbon for TEM morphological observation.

RESULTS AND DISCUSSION

Isothermal Melt Crystallization Analysis of PEKK(T)

The crystallization process is usually treated as two stages: a primary stage and a secondary stage. The crystallization is characterized by the temperature dependence. Assuming that the relative crystallinity increases with the crystallization time, then the Avrami equation[7,8] can be used to analyze the isothermal crystallization process of PEKK(T), as follows:

$$X(t) = -\exp[-kt^n] \tag{1}$$

$$\lg\{-\ln[1 - x(t)]\} = n \lg t + \lg K \tag{2}$$

The double logarithmic plot of $\lg\{-\ln[1 - x(t)]\}$ versus $\lg t$ from five different temperatures, 340, 342, 344, 346, and 348°C, is shown in Figure 1. We can observe that, for the pure Form I of PEKK(T), each curve shows an initial linear portion, then gradually tends to level off. This fact indicates the existence of a secondary crystallization process of Form I for PEKK(T), with the deviation due to the secondary crystallization being caused by the impingement of crystals in the latter crystallization process.[9,10] The values of n and k can be determined from the linear portion in Figure 1 and is shown in Table I, together with the values of the crystallization half-time $t_{1/2}$, the rate of crystallization G, and $t_{\max}$, which are defined, respectively, as the time at which the extent of crystallization is 50%, the reciprocal of $t_{1/2}$, and the necessary time for the maximum crystallization rate. The Avrami exponent n ranges from 2.33–2.69 depending upon the crystallization temperature T_c and the results indicate that the crystals in the initial stage grow in two dimensions controlled by thermal nucleation. The values of the crystallization rate parameter k increase with decrease of the crystallization temperature T_c (Table I), which indicates that PEKK(T) exhibits a very different temperature dependency, characteristic of nucleation-controlled and thermal-activated crystallization associated with proximity of the T_m and T_g, respectively.

The observations on the morphology and ED also give the same result, which indicates that apparent lamellae and single crystal-like electron diffraction, which can be indexed by Form I, are usually obtained for PEKK(T) crystallized isothermally from the melt above 310°C. The direction of the molecular chain which corresponds to the crystallographic c axis is usually inclined to the normal substrate, with an angle of 25.7°, while the a axis and b axis of the unit cell are perpendicular to c, and b is transverse to a.

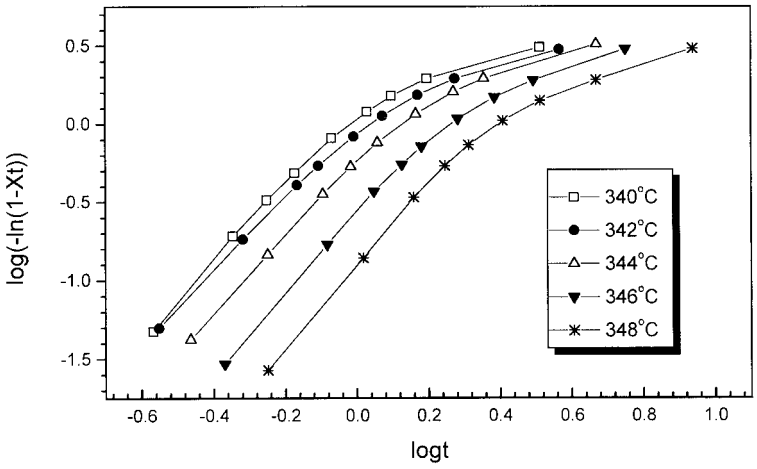

Figure 1 Plots of $\lg\{-\ln[1 - X(t)]\}$ versus $\lg t$ for isothermal crystallization from the melt for PEKK(T) at the indicated temperature.

The lamellar thickness is also measured by coating samples with Pt/Au, and the results are shown in Figure 2. The conclusion can be made that lamellar thickness increases with increased crystallization temperature. The morphology and ED for PEKK(T), crystallized isothermally from the melt at 340°C for 2 h, are shown in Figure 3, and thinner lamellae can be seen from it. Figure 4 shows the morphology observation and ED of PEKK(T) crystallized isothermally from the melt at 348°C for 2 h, which indicates that the lamellar thickness obtained from isothermal crystallization at 348°C is much larger than that at 340°C and crystals grow more perfectly at a higher crystallization temperature or with lower supercooling. The reason may be attributed to the difference between the folding energy σ and surface energy σ_e and this lamellar thickening can reduce the surface energy. The increase in lamellar thickness and improvement of the perfection result mainly from, and are decided by, lowered supercooling, not the crystallization temperature, and meanwhile, as a consequence, the melting point is usually increased.[11]

Nonisothermal Melt Crystallization Analysis of PEKK(T)

The DSC curves for crystallization exothermic peaks of PEKK(T) from the melt versus temperature at five various cooling rates Φ, 5, 10, 15, 20, and 25°C/min, are shown in Figure 5. The peak temperature T^*, where the crystallization rate is at a maximum, is shifted to a low-temperature region with the cooling rate increased (Table II). The t_{max} needed for attaining the maximum crystallization rate at different cooling rates increases with decreasing cooling rates and depends on the cooling rates. The crystallization enthalpies are also listed in Table II. The relative crystallinities $X(t_{max})$ corresponding to the t_{max}, obtained from the plots of relative crystallinity versus crystallization time t (Fig. 6), are also listed in Table II, and the results show that the crystallinity $X(t_{max})$ decreases with the cooling rate and is not more than 50%.

Assuming that the crystallization temperature is constant, we can analyze the nonisothermal

Table I Avrami Parameters n, K, $t_{1/2}$, t_{max}, $\Gamma_{1/2}$, and $X(t_{max})$ from the Avrami Equation for PEKK(T) Crystallized Isothermally from the Melt

T_c (°C)	n	K (min^{-1})	$t_{1/2}$ (min)	t_{max} (min)	$\Gamma_{1/2}$ (min^{-1})	$X(t_{max})$ (%)
340	2.48	1.30	0.77	0.73	1.29	0.449
342	2.33	0.99	0.86	0.79	1.16	0.435
344	2.42	0.58	1.09	1.01	0.93	0.444
346	2.58	0.27	1.44	1.37	0.69	0.458
348	2.69	0.13	1.89	1.82	0.53	0.466

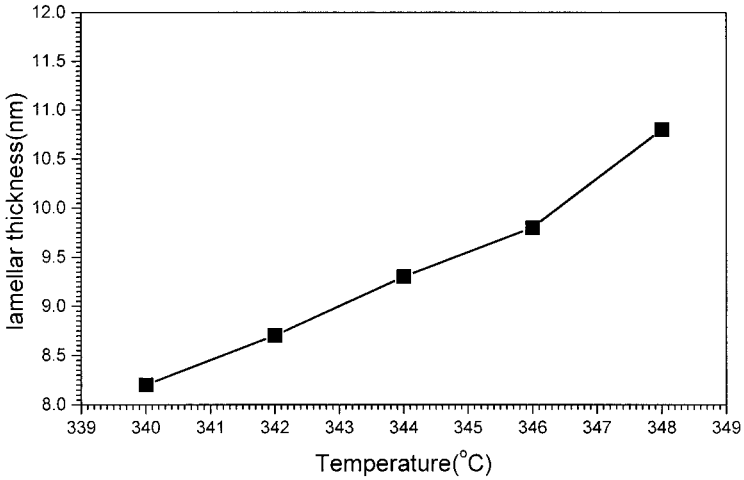

Figure 2 Plot of lamellae thickness versus crystallization temperature T_c.

crystallization process by using the Avrami equation, as proposed by Mandelkern,[12] as follows:

$$1 - X(t) = \exp[-Z_t t^n] \tag{3}$$

$$\mathrm{Lg}\{-\ln[1 - X(t)]\} = n \lg t + \lg Z_t \tag{4}$$

where Z_t is the crystallization rate constant and n is the Avrami exponent relative to the crystallization temperature T_c. Considering the dependence of Z_t on the cooling rate Φ, the final form of the crystallization rate parameters should be given as follows:

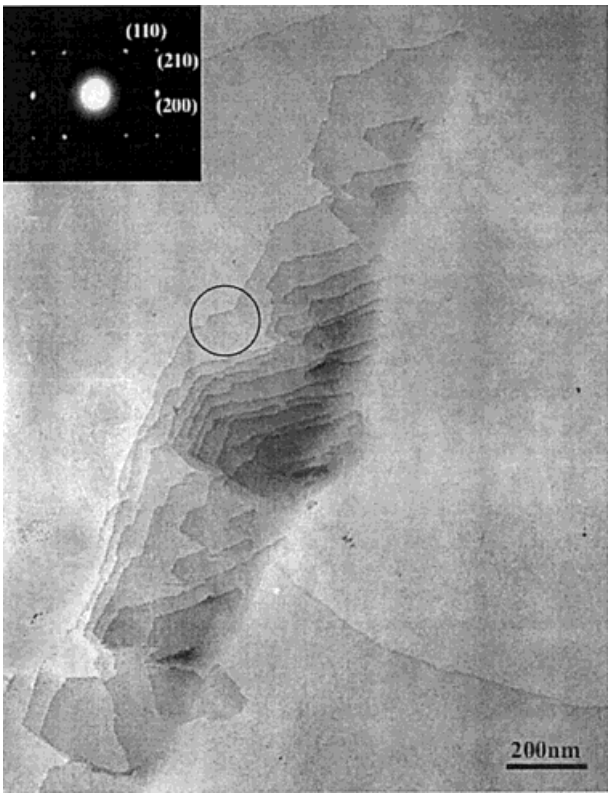

Figure 3 TEM and ED patterns for PEKK(T) crystallized isothermally from the melt at 340°C for 2 h.

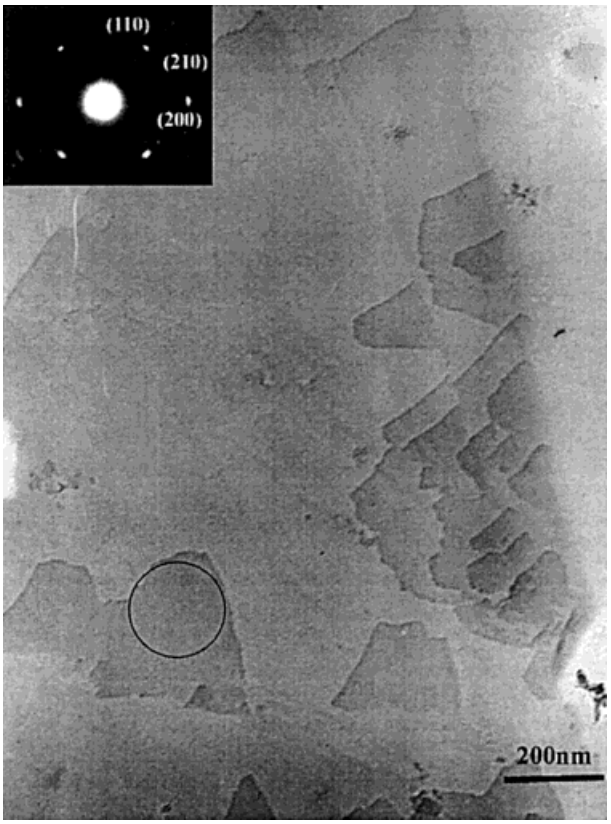

Figure 4 TEM and ED patterns for PEKK(T) crystallized isothermally from the melt at 348°C for 2 h.

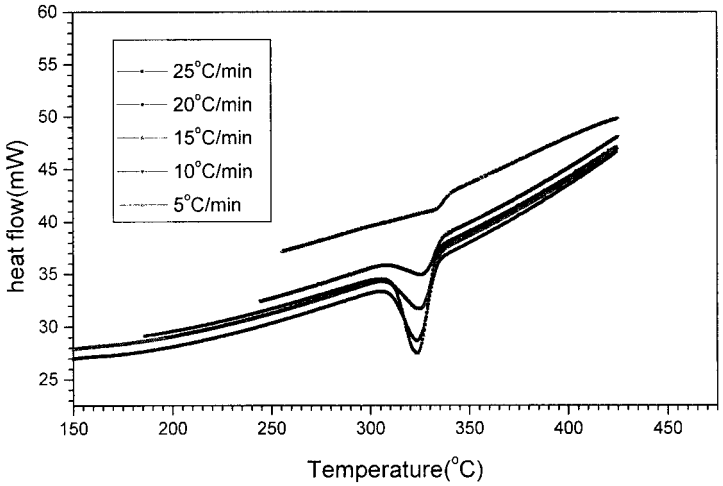

Figure 5 Plot of heat flow versus temperature for PEKK(T) from the melt at indicated cooling rate.

$$\mathrm{Lg}\ Z_c = \lg Z_t/\Phi \tag{5}$$

Drawing a plot of $\log\{-\ln(1 - X(t))\}$ versus lg t (Fig. 7), we obtain the values of the Avrami parameters n, from the slope and the rate constant Z_t or Z_c, from the intercept (Table III). Meanwhile, we obtain $t_{1/2}$, as mentioned above. These curves from the Avrami equation indicate that there are two distinct crystallization processes, the primary crystallization and the secondary crystallization, so that we have two sets of Avrami parameters and $t_{1/2}$ (Table III). Apparently, the values of the Avrami exponent n and rate constant k from the first crystallization process are much larger than is the secondary, where n_1 = 3.61–5.30 indicates that the mode of nucleation and growth at the primary process is more complicated than for the isothermal crystallization process and the former usually grows in three-dimensional extensions. However, n_2 = 2.28–3.04 at the secondary stage is more typical of the isothermal crystallization process, perhaps due to a decreased crystallization rate resulting from the impingement of spherulites at a later crystallization stage.

Spherulite morphology is usually obtained by TEM observation on PEKK(T) crystallized nonisothermally from the melt, and the size of spherulites obtained at various cooling rates can also be measured as shown in Figure 8, which indicates that, with an increasing cooling rate, the radius of the spherulites decreases accordingly. This also shows the dependence of the spherulite size on the cooling rate. Figure 9 shows the morphological observation of PEKK(T) crystallized from the melt at a 5°C/min cooling rate and indicates that the spherulites crystallized un-

Table II Values of Φ (°C/min), T^* (°C), t_{max} (min), $X(t_{max})$ (%), and ΔH (J/g)

Φ (°C/min)	T^* (°C)	t_{max} (min)	$X(t_{max})$ (%)	ΔH (J/g)
5	332.776	2.952	45.68	−41.334
10	326.222	1.932	41.51	−40.478
15	324.730	1.203	41.25	−41.514
20	323.238	0.999	41.02	−41.331
25	322.719	0.829	33.16	−42.439

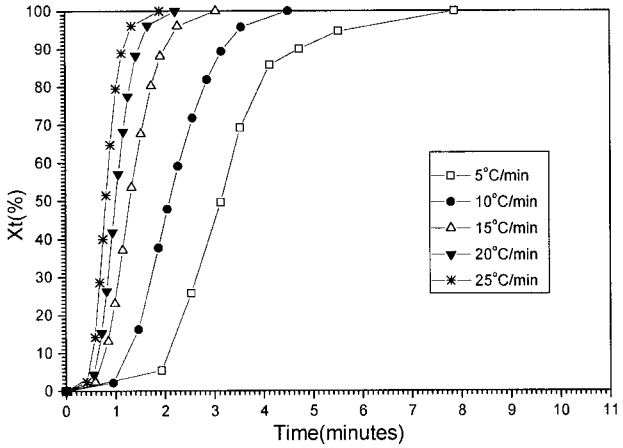

Figure 6 Plot of relative crystallinity versus time for PEKK(T) from the melt at indicated cooling rate.

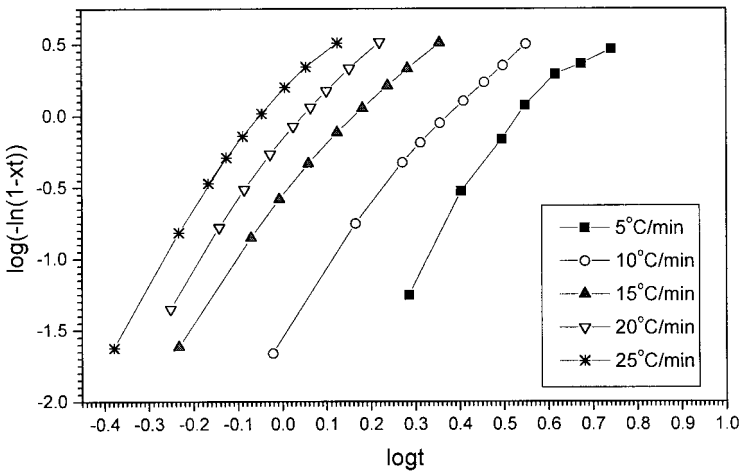

Figure 7 Plot of $\log\{-\ln[1 - X(t)]\}$ versus $\log t$ for PEKK(T) from the melt at indicated cooling rate.

der this condition possess a larger size and thicker spherulite lamellae than at a 25°C/min cooling rate, as shown in Figure 10. The reflections on the ED pattern in Figures 9 and 10 can be indexed by the unit cell parameters of Form I and show that PEKK(T) possesses Form I when crystallized nonisothermally from the melt and, moreover, that it possesses the common significant characteristics of spherulitic lamellae like other poly(aryl ether ketone)s, in which the radial growth direction of these PEKK(T) spherulites corresponds to the crystallographic *b* axis, while the unit cell axis, *a*, corresponds to transverse growth, such as the PEEK reported by Lovinger and Davis,[13–15] for which they have found similar long and narrow lamellae.

The differences in the size and perfection may be attributed to the difference in the nucleation number formed in the initial cooling stage at various cooling rates. The increased nucleation number at a higher cooling rate can increase the possibility of impingement among the spherulites, therefore resulting in more defects and a smaller spherulite size. It is the impingement of the spherulites that gives rise to the deviation from the Avrami curves in the late crystallization process and the further occurrence of two different crystallization stages.

The same analysis is also made from the plot of the relative crystallinity versus the crystallization time shown in Figure 6, which shows apparent lengthening in the induction time at a 5°C/min cooling rate compared to 25°C/min and correspondingly results in a lower nucleation number and larger size spherulites.

CONCLUSIONS

The study of the isothermal and nonisothermal crystallization on PEKK(T) was carried out by

Table III Avrami Parameters *n* and *K* from the Avrami Equation and $t_{1/2}$, t_{max}, and $X(t_{max})$ from Relation Curves of Heat Flow Versus Time and Relative Crystallinity Versus Time

	First Crystallization Stage				Second Crystallization Stage			
Γ (°C/min)	n_1	Z_{t1}	Z_{c1}	$t_{1/2}$ (min)	n_2	Z_{t2}	Z_{c2}	$t_{1/2}$ (min)
5	3.61	0.01	0.34	3.943	2.28	0.02	0.47	4.372
10	4.45	0.03	0.70	2.043	2.81	0.09	0.79	2.058
15	4.43	0.28	0.92	1.232	2.70	0.36	0.93	1.270
20	4.86	0.77	0.99	0.977	3.00	0.74	0.98	0.978
25	5.30	2.51	1.04	0.784	3.04	1.41	1.01	0.791

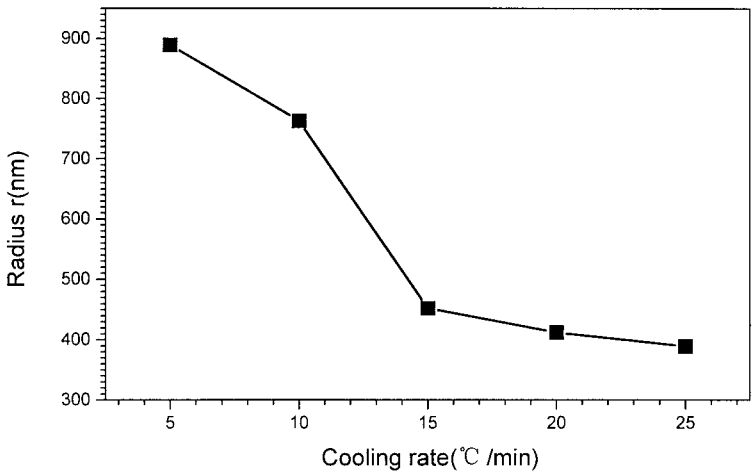

Figure 8 Plot of spherulitic radius versus cooling rate.

DSC and TEM. The Avrami analysis of isothermal melt crystallization kinetics for PEKK(T) indicates that the crystallization process is composed of a primary stage and a secondary stage. The Avrami exponent $n = 2.33–2.69$ shows that crystal growth is in two-dimensional extensions, consistent with our morphological observation, and that the single lamellar thickness increases with decreased supercooling.

For the nonisothermal melt crystallization, the results are more complicated: Analysis from the modified Avrami equation shows that there are two different crystallization processes. The

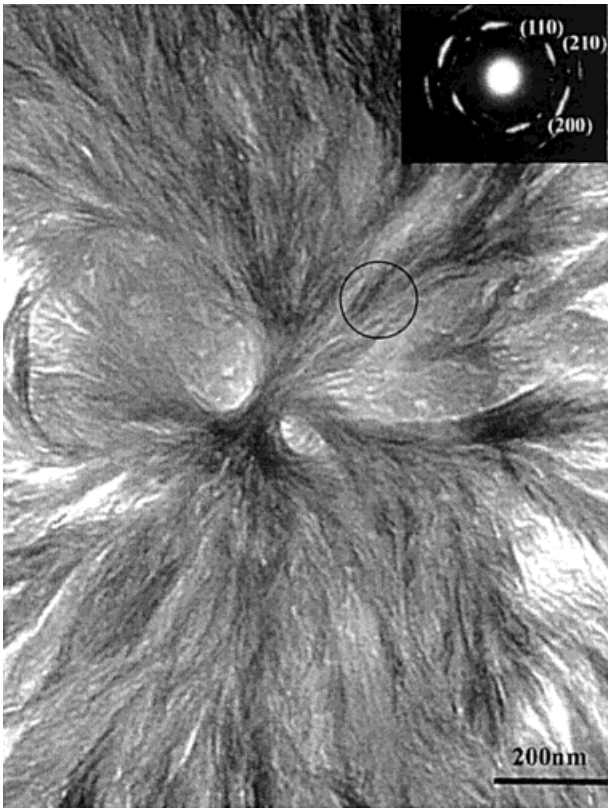

Figure 9 TEM and ED patterns for PEKK(T) crystallized nonisothermally from the melt at 5°C/min.

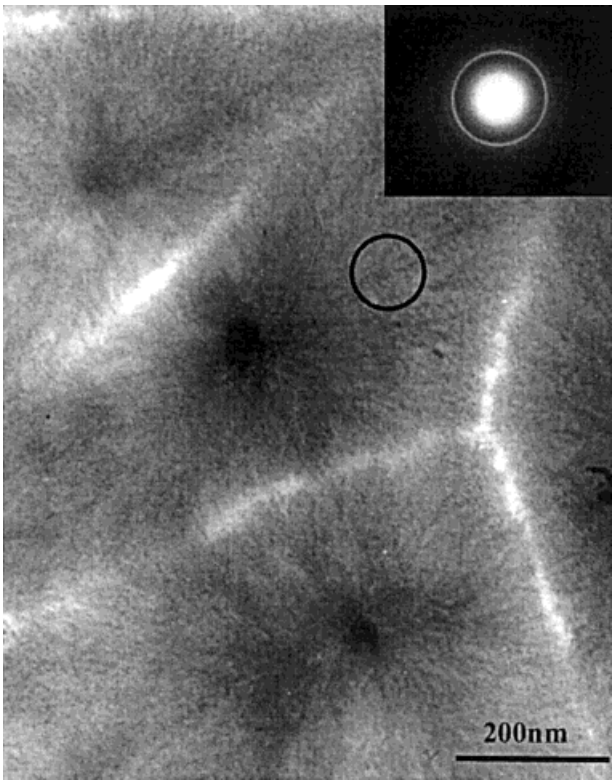

Figure 10 TEM and ED patterns for PEKK(T) crystallized nonisothermally from the melt at 25°C/min.

Avrami parameters n, 3.61–5.30, in the primary stage of the two crystallization stages, are larger than are those from the isothermal crystallization process, which indicates that the process of crystal nucleation and growth is a three-dimensional, spherulitic process. The Avrami exponent $n = 2.28–3.04$ at the secondary stage is more typical of the isothermal crystallization process, because of the decrease of the crystallization rate under the impingement and interference of crystals in the latter stage. This result is also verified by our morphological observations and ED experiments, which indicate that the size and perfection of spherulites decrease with the cooling rate, due to the difference in the nucleation number formed in the initial cooling stage at various cooling rates and the possibility of impingement among the spherulites in the subsequent crystallization process.

The authors thank the National Key Projects for Fundamental Research, "Macromolecular Condensed State," of the State Science and Technology Commission of China, and the National Natural Science Foundation of China for Funding. This work was also subsidized by the Special Funds for Major State Research Projects. The authors are very grateful to Pr. Stephen Z. D. Cheng for kindly providing the samples.

REFERENCES

1. Ho, R.; Cheng, S. Z. D.; Hsiao, B. S.; Gardner, K. H. Macromolecules 1994, 27, 2136.
2. Blundell, D. J.; Newton, A. B. Polymer 1991, 32, 308.
3. Gandner, K. H.; Hsiao, B. S.; Matheson, R. R.; Wood, B. A. Polymer 1992, 33, 2484.
4. Ho, R.; Cheng, S. Z. D.; Fisher, H. P.; Eby, R. K.; Hsiao, B. S.; Gardner, K. H. Macromolecules 1994, 27, 5787.
5. Ho, R.; Cheng, S. Z. D.; Hsiao, B. S.; Gardner, K. H. Macromolecules 1995, 27, 1938.
6. Hsiao, B. S.; Ho, R.; Cheng, S. Z. D. J Polym Sci Part B Polym Phys 1995, 33, 2439.
7. Avramim, M. J Chem Phys 1939, 15, 33.
8. Avramim, M. J Chem Phys 1940, 8, 212.
9. Wunderlich, B. Macromolecular Physics; Academic: New York, 1977; Vol. 2.
10. Liu, J. P.; Mo, Z. S. Chin Polym Bull 1991, 4, 199.
11. Sanchez, I. C.; Colson, J. P.; Eby, R. K. J Appl Phys 1973, 44, 4332.
12. Fara, R. A. Methods of Experimental Physics; Vol. 16B-Polymers, Part B: Crystal Structure and Morphology; Academic: New York, 1980.
13. Lovinger, A. J.; Davis, D. D. J Appl Phys 1985, 58, 2843.
14. Lovinger, A. J.; Davis, D. D. Macromolecules 1985, 26, 322.
15. Lovinger, A. J.; Davis, D. D. Macromolecules 1986, 19, 1861.